Laser and Particle Beams (2008), *26*, 241–248. Printed in the USA.

doi:10.1017/S0263034608000281

Proton probing measurement of electric and magnetic fields generated by ns and ps laser-matter interactions

L. ROMAGNANI,[1] M. BORGHESI,[1] C.A. CECCHETTI,[1] S. KAR,[1] P. ANTICI,[2,11] P. AUDEBERT,[2] S. BANDHOUPADJAY,[3] F. CECCHERINI,[4] T. COWAN,[5] J. FUCHS,[2] M. GALIMBERTI,[6] L.A. GIZZI,[6] T. GRISMAYER,[7] R. HEATHCOTE,[3] R. JUNG,[10] T.V. LISEYKINA,[4] A. MACCHI,[4,9] P. MORA,[7] D. NEELY,[3] M. NOTLEY,[3] J. OSTERHOLTZ,[10] C.A. PIPAHL,[10] G. PRETZLER,[10] A. SCHIAVI,[11] G. SCHURTZ,[8] T. TONCIAN,[10] P.A. WILSON,[1] AND O. WILLI[10]

[1]School of Mathematics and Physics, The Queen's University of Belfast, Belfast, UK
[2]Laboratoire pour l'Utilisation des Lasers Intenses (LULI), UMR 7605 CNRS-CEA-Ecole Polytechnique-University, Palaiseau, France
[3]Central Laser Facility, Rutherford Appleton Laboratory, Chilton, Didcot, UK
[4]Dipartimento di Fisica "E. Fermi," Università di Pisa, Pisa, Italy
[5]Physics Department, MS-220, University of Nevada, Reno, Nevada
[6]Intense Laser Irradiation Laboratory, IPCF-CNR, Pisa, Italy
[7]Centre de Physique Theorique, UMR 7644, CNRS-Ecole Polytechnique, Palaiseau, France
[8]Centre d'Etudes des Lasers Intenses et Applications, UMR 5107 Universtity of Bordeaux I-CNRS-CEA, France
[9]PolyLAB, CNR-INFM, Pisa, Italy
[10]Institut für Laser und Plasma Physik, Heinrich-Heine-Universität Düsseldorf, Germany
[11]Dipartimento di Energetica, Università di Roma, La Sapienza, Roma, Italy

(RECEIVED 12 January 2008; ACCEPTED 12 March 2008)

Abstract

The use of laser-accelerated protons as a particle probe for the detection of electric fields in plasmas has led in recent years to a wealth of novel information regarding the ultrafast plasma dynamics following high intensity laser-matter interactions. The high spatial quality and short duration of these beams have been essential to this purpose. We will discuss some of the most recent results obtained with this diagnostic at the Rutherford Appleton Laboratory (UK) and at LULI - Ecole Polytechnique (France), also applied to conditions of interest to conventional Inertial Confinement Fusion. In particular, the technique has been used to measure electric fields responsible for proton acceleration from solid targets irradiated with ps pulses, magnetic fields formed by ns pulse irradiation of solid targets, and electric fields associated with the ponderomotive channelling of ps laser pulses in under-dense plasmas.

Keywords: Laser acceleration of particles; Laser channeling; Laser-plasma interaction; Plasma dynamics; Proton probing; Self generated magnetic fields

INTRODUCTION

The development of proton probing techniques has provided a very powerful tool to explore the fast dynamics of laser-produced plasmas (Borghesi *et al.*, 2002, 2005, 2007; Mackinnon *et al.*, 2004; Romagnani *et al.*, 2005). In these techniques, a laser-accelerated proton beam is employed as a charged particle probe for the electric and magnetic fields generated in laser-plasma interactions. Thanks to the high quality of such proton probes, and in particular to their high degree of laminarity (Borghesi *et al.*, 2004; Cowan *et al.*, 2004), short burst duration and broad spectral content, detailed (spatial resolution in the μm range) time-resolved (temporal resolution in the ps range) maps of the fields and charge density and/or current density distributions in the probed plasma can be obtained (Borghesi *et al.*, 2002, 2005, 2007; Mackinnon *et al.*, 2004; Romagnani *et al.*, 2005). We present here the results of experimental investigations of laser-produced plasmas, carried on employing proton probing techniques, in a number of different interaction regimes and plasma conditions.

Address correspondence and reprint request to: L. Romagnani, School of Mathematics and Physics, The Queen's University of Belfast, Belfast BT7 1NN, UK. E-mail: l.romagnani@qub.ac.uk

DYNAMICS OF ELECTRIC FIELDS DRIVING THE LASER ACCELERATION OF MULTI-MEV PROTONS

The acceleration of multi-MeV ion beams following the interaction of short ($t_l \sim 1$ ps or less) and intense ($I_l > 10^{18}$

W/cm^2) laser pulses with thin solid foils has been one of the most active areas of research in high field science in the last few years (Clark *et al.*, 2000; Maksimchuk *et al.*, 2000; Snavely *et al.*, 2000; Flippo *et al.*, 2007; Yin *et al.*, 2006; Karmakar *et al.*, 2007). The high brightness, multi-MeV energy spectral cut-off and the excellent degree of collimation and laminarity (Borghesi *et al.*, 2004; Cowan *et al.*, 2004) distinguish these ion beams from those observed in earlier works (Gitomer *et al.*, 1986), making them suitable for a range of applications (Mackinnon *et al.*, 2004; Patel *et al.*, 2003; Santala *et al.*, 2001; Roth *et al.*, 2001). However the optimization of these ion beams for the different proposed applications requires a full understanding of the physical mechanisms involved in the acceleration process.

At the laser intensity regime achievable with modern chirped pulse amplification (CPA) lasers ($I \sim 10^{18}$–10^{21} W/cm^2) high energy protons, mainly originating from contaminant layers of water vapor and hydrocarbons on the target surface (Gitomer *et al.*, 1986), are accelerated predominantly from the back of the foil (Allen *et al.*, 2004; Fuchs *et al.*, 2005) and are emitted in the forward direction. According to the target normal sheath acceleration (TNSA) model a fraction of the laser energy is first converted into relativistic electrons at the front surface of the target. After propagating through the target, these electrons form a dense electron plasma sheath at the rear target surface. The electric field in the plasma sheath, which can be on the order of a few TV/m, ionizes the back of the target and rapidly accelerates ions normal to the initially unperturbed surface. After this initial phase, the acceleration proceeds as a plasma expansion into a vacuum (Betti *et al.*, 2005; Mora, 2003, 2005). Electrons form a Debye sheath at the front of the ion beam, and the associated space-charge separation results in a peak of the accelerating electric field at the ion front. As the beam expands, the fast electrons progressively transfer their energy to the ions and the accelerating field decreases until the acceleration ceases.

In this Section, we present the direct experimental measurement of the electric fields driving the acceleration of high energy protons from a thin foil irradiated by an intense and short laser pulse (Romagnani *et al.*, 2005). The measurement was performed employing an auxiliary laser accelerated proton beam as a transverse charged particle probe both in the proton imaging and proton deflectometry arrangements (Borghesi *et al.*, 2002, 2005, 2007; Mackinnon *et al.*, 2004; Romagnani *et al.*, 2005). The spatial structure and time evolution of the observed fields support the TNSA model. Most notably the electric field due to the initial electron sheath and the predicted field peak at the expanding ion front are detected and measured experimentally.

The experiment was carried out employing the LULI 100 TW system. A sketch of the experimental setup is shown in Figure 1a. A first 1.5 ps long CPA_1 laser pulse was focused onto 10 to 40 μm thick aluminum and gold foils (*interaction target*) at an intensity of $\sim 3.5 \times 10^{18}$ W/cm^2. A second 300 fs long CPA_2 pulse was focused onto a 10 μm thick gold foil (*proton target*) at an intensity of $\sim 2 \times 10^{19}$ W/cm^2. A proton beam was accelerated from each target and detected employing two stacks of radiochromic films (RCFs). The proton beam from the proton target was employed as a transverse charged particle probe for the electric fields at the back of the interaction target. The multi-layer arrangement of the detector provided a temporal multi-frame capability for the proton probe line within a single laser shot (Borghesi *et al.*, 2002, 2005, 2007; Mackinnon *et al.*, 2004; Romagnani *et al.*, 2005). The interaction targets were bent in order to minimize the deflections due to global target charge-up (Borghesi *et al.*, 2002; Romagnani *et al.*, 2005), which would have prevented sampling of the accelerating fields. In the proton deflectometry arrangement a metal mesh was additionally inserted between the proton target and the interaction target in order to pre-imprint a periodical pattern across the proton beam cross section (Borghesi *et al.*, 2002, 2005, 2007; Mackinnon *et al.*, 2004; Romagnani *et al.*, 2005).

In Figures 1b to 1g, typical proton imaging data are shown. In the images darker regions correspond to higher proton densities in the probe beam cross section. Each frame corresponds to a different proton probing time. Two qualitatively different structures can be seen developing in time. Around the peak of the interaction of CPA_1 with the bent foil ($t = 0$) a transient, pronounced deflection of the probe protons is observed (Fig. 1c). The probe protons are deflected away from the interaction target rear surface and are re-distributed over a bell shaped extended region (dark region indicated by an arrow in Fig. 1c). This deflection vanishes after a few ps, as can be seen by comparing Figures 1c to 1d. At later times, a front expanding from the back of the interaction target is observed. The front is delimited by a bell-shaped thin region of proton accumulation (dark line indicated by an arrow in Fig. 1e). Behind the front the probe proton density is not significantly perturbed.

We interpret this data in the framework of the TNSA model. The initial transient deflection (Fig. 1c) can be attributed to the predicted strong electric field associated with the initial dense and hot electron sheath at the rear target vacuum interface. In the same framework, the pattern observed at later times (Figs. 1d to 1g) relates to the predicted expanding proton front. The piling-up of the probe protons at the expanding front is due to the sudden drop of the electric field ahead of the front (Betti *et al.*, 2005; Mora, 2003, 2005). The fact that the probe proton density behind the front is not significantly perturbed suggests a nearly constant field in this region (Betti *et al.*, 2005; Mora 2003, 2005).

These results were confirmed by proton deflectometry measurements. In proton deflectograms (Fig. 1h), the bell-shaped expanding front observed at late probing times is marked by a clear and sudden shift of the mesh imprint lines. Note that the vertical lines remain nearly straight behind the front and that the shift along the x axis has a peak in correspondence with the front position (see also

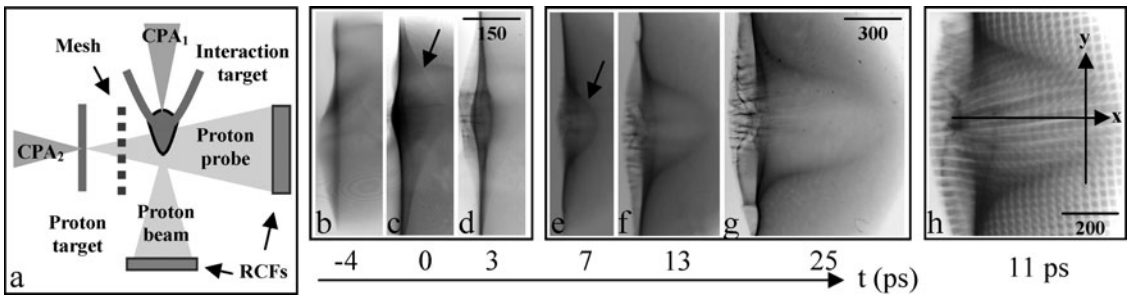

Fig. 1. (**a**) Experimental setup. (**b**–**g**) Typical proton images at different probing times ($t = 0$ corresponding to the arrival time of CPA_1). (**h**) typical proton deflectometry data. All the scales refer to the interaction target plane.

Fig. 2d, scatter graph). Such a deflection pattern reveals an electric field which peaks at the front and is uniform and substantially smaller behind it.

The experimentally measured velocity of the expanding front (Figs. 1d to 1 g) is ~3–4 × 10^7 m/s, which is consistent with the detected high energy spectral cut-off of ~6–7 MeV of the proton beam emitted from the interaction target. The expansion velocity and spectral cut-off decrease consistently when the thickness of the interaction target increases, as expected since for thicker targets the spread of the hot electrons within the target will increase, resulting in a reduced sheath electron density and therefore in a smaller accelerating field. The front velocity at different emission angles is consistent with a laminar flow. The front gains ~70% of the final velocity in the first ~2 ps after the interaction, due to the field associated with the initial electron sheath. Only ~30% of the final velocity is acquired at later times in the plasma expansion process. Note that this justifies one-dimensional (1D) models for ion acceleration, as the acceleration has practically already ceased before the transverse size of the ion front becomes comparable to the longitudinal (i.e., in the front propagation direction) size. We compared the experimental results with simulations of collisionless thin plasma expansion into a vacuum. The simulations were carried out with the 1D relativistic and electrostatic particle in cell (PIC) code and the 1D fluid code described in (Betti *et al.*, 2005; Mora; 2003, 2005). The codes take into account that the amount of energy available in the thin foil is finite, leading to a well defined cut-off in the ion energy spectrum. The simulations were initialized by estimating the initial electron temperature T_{e0} ~ 500 keV from the electron ponderomotive energy in the laser field, and the initial electron density $n_{e0} \sim 3 \times 10^{19}$ cm^{-3} from energy flux conservation. With these prescriptions the simulated expanding front dynamics and the cut-off in the ion energy spectrum resulted in very good agreement with the experiment. Figure 2a shows the electric field profile from the simulations at different times. Note the initial field peaking at the foil surface, and that at later times the field peak progressively decreases and moves together with the ion front, while a region of nearly constant field is observed behind the front.

The proton deflections in given time-dependent electric field configurations were calculated with a three-dimensional (3D) charged particle tracer (Romagnani *et al.*, 2005). In particle tracing simulation, the deflection undergone by protons propagating through a given time dependent field distribution are calculated. The geometry of the simulation fully reproduces the typical proton probing experimental set-up. Both imaging and deflectometry data were simulated. The spatial dependence (suitably extended to a 3D geometry) and the

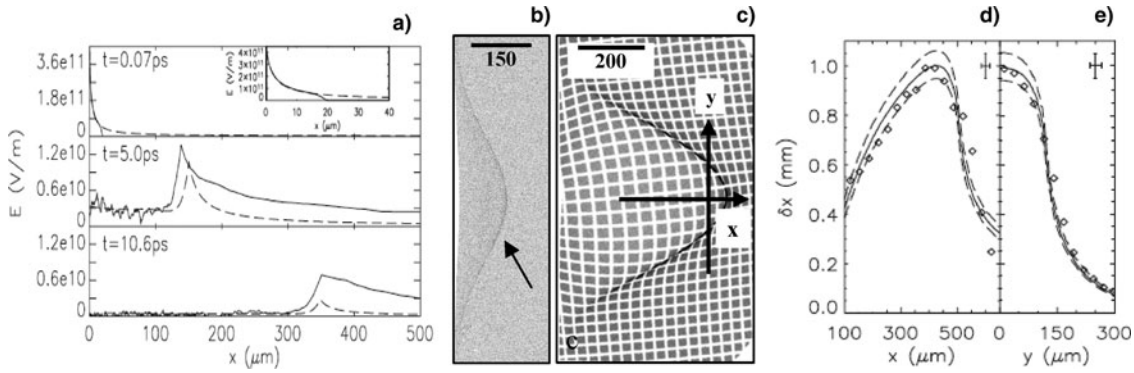

Fig. 2. (**a**) Field profiles at different times as obtained from PIC (solid line) and fluid (dashed line) simulations. (**b**) Particle tracing simulation of the initial transient field (see (**c**) Particle tracing simulation of the expanding late times front (see Fig. 1h). All the scales refer to the interaction target plane. (**d**–**e**) Comparison between the experimentally measured proton deflection (scatter graph) and the proton deflection observed in the particle tracing (line graphs).

temporal evolution of the electric field were chosen to reproduce the main features observed in the PIC and fluid simulations. We first simulated the deflection in the transient field corresponding to the case of Figure 1c. The result from the particle tracing is shown in Figure 2b. The experimental data could be best reproduced by assuming a field which is null at distances from the target larger than h, with $h \sim 20$ μm giving the best match. This seems to indicate that the electron cloud, and hence the electric field, have a finite extension, as also suggested in Passoni (2004). The best match with the experiment was found for a peak field of $\sim 4-5 \times 10^{11}$ V/m, in good agreement with the values from PIC and fluid simulations.

We then simulated the field associated with the expanding ion front, corresponding to the case of Figure 1h. The result is shown in Figure 2c. In Figures 2d to 2e, a direct comparison between the mesh line displacement in the experiment and the proton deflection observed in the simulation along the x and y axes indicated in Figures 1h and Figure 2c is also shown. The best match with the experiment at $t \sim 11$ ps was found for a field of $\sim 2-3 \times 10^9$ V/m at peak and of $\sim 10^8$ V/m in the plateau region, in good agreement with the values from PIC and fluid simulations. It is important to notice that the experiment could only be reproduced with a field which peaks at the expanding front and is constant behind it.

PROTON DEFLECTOMETRY MEASUREMENTS OF LARGE SELF-GENERATED MAGNETIC FIELDS

Precise measurements of the spatial and temporal behavior of self-generated magnetic fields (B fields) in plasmas (Stamper, 1991) are of importance for fundamental physics studies as well as inertial confinement fusion (ICF) applications (Lindl *et al.*, 2004). The evaluation, in computational codes, of B-fields and of their effect on transport is a challenge presently faced by ICF theoreticians (Nicolai *et al.*, 2000). The measurements of laser-produced magnetic fields in ICF-relevant conditions (up to the order of 10^2 T, or 1 MG), has been limited up to now to low-density (up to $\sim 10^{20}$ electron cm^{-3}) coronal plasmas where $\nabla T_e \times \nabla n_e$ B-fields have been detected by the use of optical polarimetry (Borghesi *et al.*, 1998; Stamper, 1991; Willi *et al.*, 1981). In ultra-high intensity interactions, very large B-fields ($>10^4$ T) have been revealed *via* polarization changes induced on self-generated high-harmonics (Tatatrakis *et al.*, 2002). However this technique does not provide spatially and temporally resolved field maps and cannot be applied to moderate intensity, ICF-relevant interactions.

In this Section, we present measurements of B-fields using a proton deflectometry (Borghesi *et al.*, 2005, 2007; Mackinnon *et al.*, 2004; Romagnani *et al.*, 2005) technique employing laser-accelerated protons, capable of accessing a wide range of densities, from solid density down to the tenuous coronal plasma. The magnetic fields were self-generated as a result of the interaction between a ns pulse, high-power laser with a thin Al flat solid foil. We demonstrate here unambiguously that the fields probed by the protons are magnetic by showing an inversion of the proton deflection pattern when the proton probing direction is reversed (*magnetic lens effect*), and by carrying out simultaneous transverse and axial probing on the *same* plasma. Our experimental measurements also show that the $\nabla T_e \times \nabla n_e$ term is the dominant magnetic field source and that the fields produced in the dense plasma zone, beyond the critical density region, are at least one order of magnitude lower than the amplitude of the fields in the coronal region.

The experiment was performed at the Rutherford Appleton Laboratory (RAL) using the Vulcan Nd:glass laser. A sketch of the experimental set-up is shown in Figures (3a and 3b). Targets consisting of 6 μm thick Al foils were irradiated with 50 J, 1 ns duration laser pulses at on-target intensities in the range $3-6 \times 10^{14}$ W/cm^2 in circular polarization. We alternatively irradiated the front and back surface of the target, in separate shots with two such beams. Two proton probe beams (up to 15 MeV in energy), accelerated by irradiating two thin Au solid foil (25 μm thick) with 50 J, 1 ps CPA laser pulses at an on-target intensity of 5×10^{19} W/cm^2, were used in the proton deflectometry arrangement to probe the plasmas produced by the ns pulse along two perpendicular probing directions.

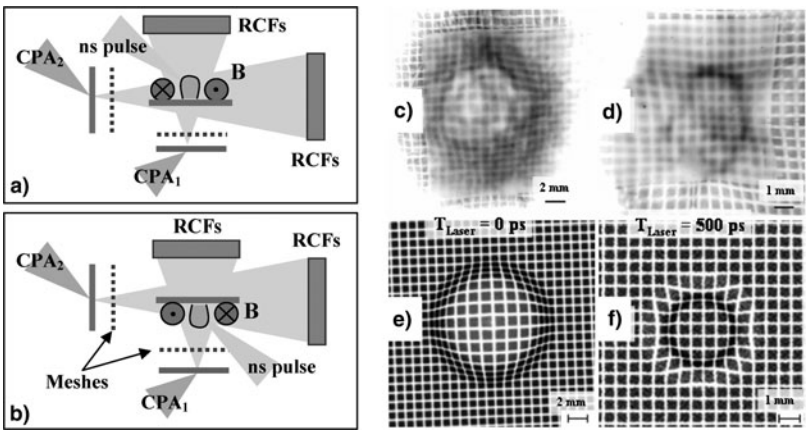

Fig. 3. (**a**–**b**) Experimental set-up in the two different configurations for the ns pulse. (**c**–**d**) Proton deflectometry data for face-on probing ((**c**) corresponding to the set-up (a)). (**e**–**f**) Particle tracing simulations ((e) corresponding to the set-up (a)).

With this setup two proton deflection maps were simultaneously obtained in each shot, one of which was *face-on* (i.e., with the proton probe axis parallel to the plasma axis) and the other one was *side-on* (i.e., with proton probe axis parallel to the target surface). Depending on which ns pulse was used, the plasma was probed by the *face-on* proton beam in two different configurations: interaction facing the incoming probing beam (*front interaction*), or interaction placed at the rear surface of the target (*rear interaction*) (see Figs. 3a and 3b). This allowed for the face-on beam to probe plasmas produced on either sides of the target and therefore to change the azimuthal direction of the magnetic field with respect to the axis of the proton probe.

Figures (3c to 3d) shows face-on deflectograms taken around the peak of the pulse in front and rear interaction configurations. As expected, due to the field azimuthal geometry, face-on radiography shows to be more sensitive to B-fields than side-on geometry. Furthermore, in face-on probing, one expects B-fields induced deflections to differ strongly in *front* and *rear interaction* configurations, due to the change in the direction of the $\mathbf{v} \times \mathbf{B}$ force acting on the probe protons. This is demonstrated by comparing Figures 2c and 2d: while in rear interactions (Fig. 2c) the magnetic field deflects outward the ions, causing the stretching of the mesh elements, in the other case (Fig. 2d), it causes a compression of the mesh lines in the inner part of the plasma. This effect is a demonstration of the presence of a magnetic field, as inverting the probing direction would not affect the transverse deflection if this was mainly caused by radial electric fields in the plasma.

The ns interaction was simulated by the MHD package of the Lagrangian code CHIC using the experimental parameters. The simulation shows two distinct magnetic field components. In the low density region of the ablating plasma, a toroidal B-field localized around 100 μm away from the expansion axis and with a maximum amplitude of 50 T is observed. This field is peaked at densities ~5–8 10^{20} cm^{-3} and extends over ~90 μm. This field component can be associated with the $\nabla T_e \times \nabla n_e$ source term. In the denser plasma (~2×10^{21} cm^{-3}) region, localized around 10 μm from the axis and extending over ~20 μm, one also observe another component of the magnetic field which is reversed and has a considerably smaller (~5 T) amplitude and a smaller extent. This field component can be associated with resonance absorption. The dominance of the coronal magnetic field over the axial one in the dense region of the plasma is consistent with the fact that resonance absorption is minimal in our experimental conditions.

A particle tracer (Schiavi, 2003) was employed to model the propagation of the probe protons through the electric and magnetic field configuration predicted by CHIC. Particle tracing simulations are shown in Figures 3e to 3f. The model magnetic field employed in the simulation has two components: one (the dense plasma component) centered on axis, and the other (the coronal plasma component) off-axis, reproducing the main features observed in CHIC simulations. An almost perfect match between experimental and simulated maps, in terms of mesh pattern deflection and dose distribution was obtained. Indeed the optimum parameters for the input fields in order to reproduce the experimental data differ from the CHIC predictions only by a factor ~10 T for the coronal B-field. We observe that the mesh patterns pre-imprinted in the proton beam are compressed or magnified in correspondence of the central part of the plasma depending on the magnetic field direction, as observed in the experiment.

DYNAMICS OF CHARGE-DISPLACEMENT CHANNELLING IN INTENSE LASER-PLASMA INTERACTIONS

The study of the propagation of intense laser pulses in underdense plasmas is relevant to several highly advanced applications, including electron (Malka *et al.*, 2005; Karmarkar *et al.*, 2007; Lifschitz *et al.*, 2006; Mangles *et al.*, 2006) and ion acceleration (Krushelnick *et al.*, 1999), development of X- and γ-ray sources (Rousse *et al.*, 2004), and fusion neutron production (Fritzler *et al.*, 2002). It is also of fundamental interest, due to the variety of relativistic and nonlinear phenomena which arise in laser-plasma interactions (Morou *et al.*, 2006). Among these, self-focusing and self-channelling of the laser pulse arise in this regime from the intensity dependence of the relativistic index of refraction and the ponderomotive expulsion of plasma from the propagation axis (Mori *et al.*, 1998). For intense pulses, charge separation effects become important and the pulse can propagate self-guided in a charged channel (Borisov, 1992). Several experiments have investigated this regime, mostly providing indirect evidence of self-channeling via optical diagnostics (Borisov *et al.*, 1992; Borghesi *et al.*, 1997).

In this Section, we report on an experiment where proton imaging techniques were applied to the study of the formation and subsequent evolution of a charge displacement channel in underdense plasma. These investigations have led to the first direct experimental detection of the transient electric fields in the channel, providing an insight of the fundamental physical processes involved. The comparison of the experimental data with 2D electromagnetic (EM) PIC simulations and a simple1D electrostatic (ES) PIC model allows a detailed characterization of the electric field dynamics at different stages of its evolution.

The experiment was carried out at the Rutherford Appleton Laboratory, employing the VULCAN Nd-Glass laser system, providing two CPA pulses. Each of the beams delivered approximately 30 J on target in 1.3 ps. The beams were focused at peak intensities up to 3×10^{19} W/cm^2. A sketch of the experimental set-up is shown in Figure 4a. One of the beams (CPA_1) was directed to propagate through He gas from a supersonic nozzle, having a 2 mm aperture, driven at 50 bar pressure. The interaction

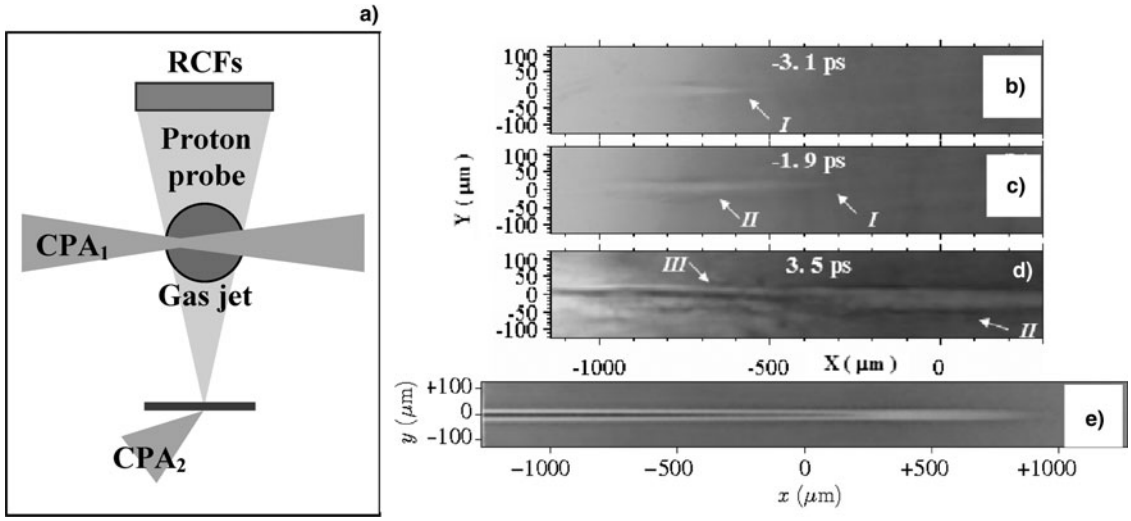

Fig. 4. (**a**) Experimental set-up. (**b**–**d**) Typical proton imaging data showing the bullet shaped front (regions I), the electron depleted channel (regions II) and the dark line indicating an electric field pointing towards the channel axis (region III). (**e**) Particle tracing simulation.

was transversely probed by the proton beam produced from the interaction of the second CPA beam (CPA_2) with a flat foil (a 10 μm thick Au foil was typically used).

Figures 4b to 4d shows time-resolved proton-projection images. Each frame corresponds to a given proton probing time, with $t = 0$ corresponding to the estimated arrival of the peak of the CPA_1 at its focal plane $x = 0$. The laser pulse propagates from left to right. A white channel with dark boundaries (Figs. 4c to 4d), regions II with a bullet shaped leading edge (Figs. 4b to 4c), regions I are clearly visible in the proton images. The channel appears to propagate along the laser axis. Its velocity, estimated by comparing frames (Fig. 4b) and (Fig. 6c), is equal to the speed of light, within the experimental error. In the trail of the channel the proton flux distribution around the axis changes qualitatively, showing a dark line along the axis (Fig. 4d, region (III)), which is observed up to tens of ps after the transit of the peak of the pulse. The white channel indicates the presence of a positively charged region around the laser axis, where the electric field points outwards, along the radial direction. The central dark line observed at later times in the channel suggests that at this stage the radial electric field points inwards in the vicinity of the axis and outwards at larger distances from it.

The main features observed in the experiment are reproduced by 2D EM and 1D ES PIC simulations. The simulation clearly shows the formation of an electron-depleted channel, resulting in an outwardly directed radial space-charge electric field whose peak value is 6.7×10^{10} V/m. In the region behind the peak of the pulse, two narrow ambipolar fronts (one on either side of the propagation axis) are observed. The ambipolar fields have peak values of ~6×10^{10} V/m. The proton dose map obtained in the experiment could be reproduced by particle tracing simulations (Schiavi, 2003) where an input field distribution matching the electric field distribution and time evolution obtained from PIC simulations was employed (Fig. 4e).

An essential description of the observed channel dynamics is suggested by the ES PIC simulations. In the first stage, the ponderomotive force (PF) pushes part of the electrons outwards. A positively charged channel along the axis is therefore formed. As a consequence a radial space charge separation field (SCSF) is created, which holds the electrons back until a balance between the PF and the SCSF is reached. Such a field also deflects the probe protons, leading to the feature observed in Figures 4c to 6d regions II. Meanwhile the SCSF accelerates the ions in the outward radial direction, producing a depression in the ion density around the axis. Even after the laser pulse ceases, the ions retain the velocity acquired during the acceleration stage. Correspondingly the fastest ions overturn the slowest ones and hydrodynamic breaking of the ion fluid occurs. An ion density peak is formed at the breaking position, away from the laser axis. Electrons are strongly heated around the ion density peak, generating a hot electron population with a temperature $T_h \sim 13$ keV and a density $n_h \sim 4 \times 10^{19}$ cm^{-3}. A simple modelling of the sheath field generated around the ion density spike (Macchi *et al.*, 2007) yields a peak field $E_s \sim 6 \times 10^{10}$ V/m, consistently with the simulation results. The ambipolar field at the breaking location can be thus be interpreted as the sheath field resulting from the local electron heating. Such an electric field deflects the probe protons, leading to the feature shown in Figure 4d region III.

ACKNOWLEDGMENTS

The authors acknowledge the support of the EU program HPRI CT 1999-0052, of Grant No. E1127 from Region Ile-de- France, UNR Grant No. DE-FC52-01NV14050, of EPSRC, of CCLRC, of Royal Society Joint Project and Short Visit Grants, of DAAD, of British

Council-MURST-CRUI, COST and INTAS Networks, of MIUR (Italy) via a PRIN project, of British Council/Alliance, ANDOR Technology, IRCEP/QUB scheme and of DFG funded programs SFB/TR18 and GK1203. Part of the simulations were performed on the Linux cluster at the CINECA facility (Bologna, Italy) sponsored by the INFM supercomputing initiative. The authors acknowledge S.V. Bulanov, F. Cornolti, and F. Pegoraro for useful discussions, and the precious assistance of the LULI and RAL laser staff.

REFERENCES

Allen, M., Patel, P.K., Mackinnon, A., Price, D., Wilks, S. & Morse, E. (2004). Direct experimental evidence of back-surface ion acceleration from laser-irradiated gold foils. *Phys. Rev. Lett.* **93**, 265004.

Betti, S., Ceccherini, F., Cornolti, F. & Pegoraro, F. (2005). Expansion of a finite-size plasma in vacuum. *Plasma Phys. Contr. Fusion* **47**, 521–529.

Borghesi, M., Mackinnon, A.J., Barringer, L., Gaillard, R., Gizzi, L.A., Meyer, C., Willi, O., Pukhov, A. & Meyer-Ter-Vehn, J. (1997). Relativistic channeling of a picosecond laser pulse in a near-critical preformed plasma. *Phys. Rev. Lett.* **78**, 879–882.

Borghesi, M., Mackinnon, A.J., Bell, A.R., Gaillard, R. & Willi, O. (1998). Megagauss magnetic field generation and plasma jet formation on solid targets irradiated by an ultraintense picosecond laser pulse. *Phys. Rev. Lett.* **81**, 112–115.

Borghesi, M., Campbell, D.H., Schiavi, A., Willi, O., Mackinnon, A.J., Hicks, D., Patel, P., Gizzi, L.A., Galimberti, M. & Clarke, R.J. (2002). Laser-produced protons and their application as a particle probe. *Laser Part. Beams* **20**, 269–275.

Borghesi, M., Mackinnon, A.J., Campbell, D.H., Hicks, D.G., Kar, S., Patel, P.K., Price, D., Romagnani, L., Schiavi, A. & Willi, O. (2004). Multi-MeV Proton Source Investigations In Ultraintense Laser-Foil Interactions. *Phys. Rev. Lett.* **92**, 055003.

Borghesi, M., Audebert, P., Bulanov, S.V., Cowan, T., Fuchs, J., Gauthier, J.C., Mackinnon, A.J., Patel, P.K., Pretzler, G., Romagnani, L., Schiavi, A., Toncian, T. & Willi, O. (2005). High-intensity laser-plasma interaction studies employing laser-driven proton probes. *Laser Part. Beams* **23**, 291–295.

Borghesi, M., Kar, S., Romagnani, L., Toncian, T., Antici, P., Audebert, P., Brambrink, E., Ceccherini, F., Cecchetti, C.A., Fuchs, J., Galimberti, M., Gizzi, L.A., Grismayer, T., Lyseikina, T., Jung, R., Macchi, A., Mora, P., Osterholtz, J., Schiavi, A. & Willi, O. (2007). Impulsive electric fields driven by high-intensity laser matter interactions. *Laser Part. Beams* **25**, 161–167.

Borisov, A.B., Borovskiy, A.V., Korobkin, V.V., Prokhorov, A.M., Shiryaev, O.B., Shi, X.M., Luk, T.S., Mcpherson, A., Solem, J.C., Boyer, K. & Rhodes, C.K. (1992). Observation Of Relativistic And Charge-Displacement Self-Channelling Of Intense Subpicosecond Ultraviolet (248 Nm) Radiation In Plasmas. *Phys. Rev. Lett.* **68**, 2309–2312.

Clark, E.L., Krushelnick, K., Davies, J.R., Zepf, M., Tatarakis, M., Beg, F.N., Machacek, A., Norreys, P.A., Santala, M.I.K., Watts, I. & Dangor, A.E. (2000). Measurements of energetic proton transport through magnetized plasma from intense laser interaction with solids. *Phys Rev. Lett.* **84**, 670–673.

Cowan, T.E., Fuchs, J., Ruhl, H., Kemp, A., Audebert, P., Roth, M., Stephens, R., Barton, I., Blazevic, A., Brambrink, E., Cobble, J., Fernandez, J., Gauthier, J.-C., Geissel, M., Hegelich, M., Kaae, J., Karsch, S., Le Sage, G.P., Letzring, S., Manclossi, M., Meyroneinc, S., Newkirk, A., Pepin, H. & Renard-Le Galloudec, N. (2004). Ultralow emittance, multi-mev proton beams from a laser virtual-cathode plasma accelerator. *Phys. Rev. Lett.* **92**, 204801.

Flippo, K., Hegelich, B.M., Albright, B.J., Yin, L., Gautier, D.C., Letzring, S., Schollmeier, M., Schreiber, J., Schulze, R. & Fernandez, J.C. (2007). Laser-driven ion accelerators: Spectral control, monoenergetic ions and new acceleration mechanisms. *Laser Part. Beams* **25**, 3–8.

Fritzler, S., Najmudin, Z., Malka, V., Krushelnick, K., Marle, C., Walton, B., Wei, M.S., Clarke, R.J. & Dangor, A.E. (2002). Ion heating and thermonuclear neutron production from high-intensity subpicosecond laser pulses interacting with underdense plasmas. *Phys. Rev. Lett.* **89**, 165004.

Fuchs, J., Sentoku, Y., Karsch, S., Cobble, J., Audebert, P., Kemp, A., Nikroo, A., Antici, P., Brambrink, E., Blazevic, A., Campbell, E.M., Fernandez, J.C., Gauthier, J.-C., Geissel, M., Hegelich, M., Pepin, H., Popescu, H., Renard-Legalloudec, N., Roth, M., Schreiber, J., Stephens, R. & Cowan, T.E. (2005). Comparison of laser ion acceleration from the front and rear surfaces of thin foils. *Phys. Rev. Lett.* **94**, 045004.

Gitomer, S.J., Jones, R.D., Begay, F., Ehler, A.W., Kephart, J.F. & Kristal, R. (1986). Fast ions and hot electrons in the laser-plasma interaction. *Phys. Fluids* **29**, 2679–2688.

Karmakar, A. & Pukhov, A. (2007). Collimated attosecond GeV electron bunches from ionization of high-Z material by radially polarized ultra-relativistic laser pulses. *Laser Part. Beams* **25**, 371–377.

Krushelnick, K., Ting, A. Moore, C.I., Burris, H.R., Esarey, E., Sprangle, P. & Baine, M. (1997). Plasma channel formation and guiding during high intensity short pulse laser plasma experiments. *Phys. Rev. Lett.* **78**, 4047–4050.

Krushelnick, K., Clark, E.L., Najmudin, Z., Salvati, M., Santala, M.I.K., Tatarakis, M., Dangor, A.E., Malka, V., Neely, D., Allot, R. & Danson, C. (1999). Multi-Mev ion production from high-intensity laser interactions with underdense plasmas. *Phys. Rev. Lett.* **83**, 737–740.

Lifschitz, A.F., Faure, J., Glinec, Y., Malka, V. & Mora, P. (2006). Proposed scheme for compact GeV laser plasma accelerator. *Laser Particle Beams* **24**, 255–259.

Lindl, J.D., Amendt, P., Berger, R.L., Glendinning, S.G., Glenzer, S.H., Haan, S.W., Kauffman, R.L., Landen, O.L. & Suter, L.J. (2004). The physics basis for ignition using indirect-drive targets on the National Ignition Facility. *Phys. Plasmas* **11**, 339–491.

Macchi, A., Ceccherini, F., Cornolti, F., Kar, S. & Borghesi, M. (2007). Ponderomotive laser ion acceleration and electric field dynamics following charge-displacement channeling. http://arxiv.org/abs/physics/0701139.

Mackinnon, A.J., Patel, P.K., Town, R.P., Edwards, M.J., Phillips, T., Lerner, S.C., Price, D.W., Hicks, D., Key, M.H., Hatchett, S., Wilks, S.C., Borghesi, M., Romagnani, L., Kar, S., Toncian, T., Pretzler, G., Willi, O., Koenig, M., Martinolli, E., Lepape, S., Benuzzi-Mounaix, A. Audebert, P., Gauthier, J.C., King, J., Snavely, R., Freeman, R.R. & Boehlly, T. (2004). Proton radiography as an electromagnetic field and density perturbation diagnostic (Invited). *Rev. Sci. Instrum.* **75**, 3531–3536.

Maksimchuk, A., Gu, S., Flippo, K., Umstadter, D. & Bychenkov, Vy. (2000). Forward ion acceleration in thin films driven by a high intensity laser. *Phys. Rev. Lett.* **84**, 4108–4111.

Malka, V., Faure, J., Glinec, Y. & Lifschitz, A.F. (2005). Laser-plasma accelerators: a new tool for science and for society. *Plasma Phys. Contr. Fusion* **47**, B481–B490.

Mangles, S.P.D., Walton, B.R., Najmudin, Z., Dangor, A.E., Krushelnick, K., Malka, V., Manclossi, M., Lopes, N., Carias, C., Mendes, G. & Dorchies, F. (2006). Table-top laser-plasma acceleration as an electron radiography source. *Laser Part. Beams* **24**, 185–190.

Mora, P. (2003). Plasma expansion into a vacuum. *Phys. Rev. Lett*. **90**, 185002.

Mora, P. (2005). Thin-foil expansion into a vacuum. *Phys. Rev. E* **72**, 056401.

Mori, W.B., Joshi, C., Dawson, J.M., Forslund, D.W. & Kindel, J.M. (1998). Evolution of self-focusing of intense electromagnetic waves in plasma. *Phys. Rev. Lett*. **60**, 1298–1301.

Morou, G.A., Tajima, T. Bulanov, S.V. (2006). Optics in the relativistic regime. *Rev. Mod. Phys*. **78**, 309–371.

Nicolai, P., Vandenboomgaerde, M., Canaud, B. & Chaigneau, F. (2000). Effects of self-generated magnetic fields and nonlocal electron transport in laser produced plasmas. *Phys. Plasmas* **7**, 4250–4258.

Passoni, M. & Lontano, M. (2004). One-dimensional model of the electrostatic ion acceleration in the ultraintense laser-solid interaction. *Laser Part. Beams* **22**, 163–169.

Patel, P.K., Mackinnon, A.J., Key, M.H., Cowan, T.E., Foord, M.E., Allen, M., Price, D.F., Ruhl, H., Springer, P.T. & Stephens, R. (2003). Isochoric heating of solid-density matter with an ultrafast proton beam. *Phys. Rev. Lett*. **91**, 125004.

Romagnani, L., Fuchs, J., Borghesi, M., Antici, P., Audebert, P., Ceccherini, F., Cowan, T., Grismayer, T., Kar, S., Macchi, A., Mora, P., Pretzler, G., Schiavi, A., Toncian, T. & Willi, O. (2005). Dynamics of electric fields driving the laser acceleration of multi-MeV protons. *Phys. Rev. Lett*. **95**, 195001.

Romagnani, L. (2005). Laser-Plasma Investigations Employing Laser-Driven Proton Probes. PhD Thesis, The Queen's University of Belfast, Belfast, UK.

Roth, M., Cowan, T.E., Key, M.H., Hatchett, S.P., Brown, C., Fountain, W., Johnson, J., Pennington, D.M., Snavely, R.A., Wilks, S.C., Yasuike, K., Ruhl, H., Pegoraro, F., Bulanov, S.V., Campbell, E.M., Perry, M.D. & Powell, H. (2001). Fast ignition by intense laser-accelerated proton beams. *Phys. Rev. Lett*. **86**, 436–439.

Rousse, A., Ta Phuoc, K.T., Shah, R., Pukhov, A., Lefebvre, E., Malka, V., Kiselev, S., Burgy, F., Rousseau, J.-P., Umstader, D. & Hulin, D. (2004). Production of a keV X-Ray beam from synchroton radiation in relativistic laser-plasma interaction. *Phys. Rev. Lett*. **93**, 135005.

Santala, M.I.K., Zepf, M., Beg, F.N., Clark, E.L., Dangor, A.E., Krushelnick, K., Tatarakis, M., Watts, I., Ledingham, K.W.D., Mccanny, T., Spencer, I., Machacek, A.C., Allot, R., Clarke, R.J. & Norreys, P.A. (2001). Production of radioactive nuclides by energetic protons generated from intense laser-plasma interactions. *Appl. Phys. Lett*. **78**, 19–21.

Schiavi, A.M. (2003). Study of Laser-Produced Plasmas by X-ray and Proton Radiography. PhD Thesis, Imperial College of Science, London, UK.

Snavely, R.A., Key, M.H., Hatchett, S.P., Cowan, T.E., Roth, M., Phillips, T.W., Stoyer, M.A., Henry, E.A., Sangster, T.C., Singh, M.S., Wilks, S.C., Mackinnon, A., Offenberger, A., Pennington, D.M., Yasuike, K., Langdon, A.B., Lasinski, B.F., Johnson, J., Perry, M.D. & Campbell, E.M. (2000). Intense high-energy proton beams from petawatt-laser irradiation of solids. *Phys. Rev. Lett*. **85**, 2945–2948.

Stamper, J.A. (1991). Review on spontaneous magnetic fields in laser-produced plasmas: Phenomena and measurements. *Laser Part. Beams* **9**, 841–862.

Tatarakis, M., Watts, I., Beg, F.N., Clark, E.L., Dangor, A.E., Gopal, A., Haines, M.G., Norreys, P.A., Wagner, U., Wei, M.-S., Zepf, M. & Krushelnick, K. (2002). Measuring huge magnetic fields. *Nature* **415**, 280.

Willi, O., Rumsby, P.T. & Duncan, C. (1981). Megagauss magnetic fields on laser irradiated spherical targets, *Opt. Commun*. **37**, 40–44.

Yin, L., Albright, B.J., Hegelich, B.M. & Fernandez, J.C. (2006). GeV laser ion acceleration from ultrathin targets: The laser break-out afterburner. *Laser Part. Beams* **24**, 291–298.